

Multiwavelength Signatures of Cosmic Ray Acceleration by Young Supernova Remnants

Jacco Vink

Astronomical Institute Utrecht, Utrecht University, P.O. Box 80000, 3508TA Utrecht, Netherlands

Abstract. An overview is given of multiwavelength observations of young supernova remnants, with a focus on the observational signatures of efficient cosmic ray acceleration. Some of the effects that may be attributed to efficient cosmic ray acceleration are the radial magnetic fields in young supernova remnants, magnetic field amplification as determined with X-ray imaging spectroscopy, evidence for large post-shock compression factors, and low plasma temperatures, as measured with high resolution optical/UV/X-ray spectroscopy. Special emphasis is given to spectroscopy of post-shock plasma's, which offers an opportunity to directly measure the post-shock temperature. In the presence of efficient cosmic ray acceleration the post-shock temperatures are expected to be lower than according to standard equations for a strong shock. For a number of supernova remnants this seems indeed to be the case.

Keywords: visible, x-rays: observations – supernova remnants: general – cosmic rays: acceleration

PACS: 95.30.Qd, 95.30.Tg, 95.85.Bh, 95.85.Kr, 95.85.Mt, 95.85.Nv, 97.60.Bw, 98.38.Mz, 98.70.Sa

INTRODUCTION

Young supernova remnants are interesting from many different points of view: they are important for studying the freshly synthesized supernova material, thereby giving clues about the supernova explosion itself [1, 2, for some recent examples], and they are of interest for many physical processes associated with low density plasmas, for example collisionless shock physics and non-equilibrium ionization. However, in keeping with the theme of this symposium, I will focus here on those multiwavelength aspects that reveal something about the cosmic ray acceleration properties of young supernova remnants (SNRs).

For a long time SNRs have been considered the prime candidates for providing the bulk of the cosmic rays observed on earth in the energy range up to $E \sim 3 \times 10^{15}$ eV (the “knee” in the cosmic ray spectrum), but possibly even up to 10^{18} eV (the “ankle”). The supernova energetics and rates are sufficient to explain the energy density of Galactic cosmic rays, but the problem was that the conditions in SNRs seemed not right for accelerating particle up to, or beyond, energies of 10^{15} eV. In particular, the magnetic field strengths and turbulence needed for fast acceleration, were considered unlikely to exist in SNRs [3].

Since the 1950-ies it is known that at least some particles get accelerated up to relativistic energies, since SNRs turned out to be sources of synchrotron radio emission, which indicated the presence of relativistic electrons [4, for an early discussion]. However, the electrons producing radio synchrotron emission have energies in the GeV range, far short of the 10^{15} eV needed to explain

the cosmic ray spectrum.

From the 1950-ies to the mid 1990-ies not much observational progress was made concerning cosmic ray acceleration by SNRs. Disappointingly, γ -ray experiments like COS-B, or EGRET revealed little evidence for the presence of high energy cosmic rays inside SNRs, although EGRET did find a possible connection between γ -ray sources and old SNRs near molecular clouds [5].

Over the last decade the situation has changed considerably. X-ray observations have shown that a) electrons are accelerated to > 10 TeV energies in some SNRs [6], b) magnetic fields in SNRs are much larger ($\gtrsim 100 \mu\text{G}$) than the compressed average field in the interstellar medium ($\sim 5 \mu\text{G}$) [e.g. 7, 8, 9, 10].

The presence of > 10 TeV electrons reveals that SNR shocks are capable of acceleration particles to very high energies, although it does not yet provide direct evidence that ions, which constitute the bulk of the cosmic rays observed on earth, are accelerated beyond 10^{15} eV.

However, the relatively high magnetic field at least indicates the conditions for accelerating particles up to 10^{15} eV are present. Moreover, the high magnetic fields probably arise through plasma wave generation by cosmic rays themselves [e.g. 11]. High magnetic fields in SNRs, therefore, provide indirect evidence for efficient cosmic ray acceleration.

Direct evidence that, indeed, ions are accelerated to high energies by young SNRs comes from TeV γ -ray observations. Several SNRs have now been detected by Cherenkov γ -ray telescopes [12, 13, 14, 15], but the interpretation of the results are hotly debated [16]: is the γ -ray emission caused by inverse Compton scattering of > 10 TeV electrons, or is it due to the decay of neutral

pions created by energetic ion-ion collisions?

Although this is an ongoing debate, we will likely make major advances in our understanding in the next decade. One of the reasons is the rapid developments in TeV astronomy, but multiwavelength data are necessary to interpret the TeV data (e.g. to estimate densities, magnetic fields), and as I will show multiwavelength observation will help to reveal whether ions are efficiently accelerated, where and when they will be accelerated, and how much of the shock energy will be taken up by cosmic rays.

SUPERNOVA REMNANT SHOCKS

Shock evolution

A typical supernova explosion blows material into the interstellar/circumstellar medium (CSM/ISM) with velocities up to 10,000-20,000 km s⁻¹, and a total kinetic energy of $\sim 10^{51}$ erg. This ejected material is initially hot from the supernova explosion itself, but due to the high expansion rate, the ejecta cool very fast, even allowing dust to condense (as detected in the SNR Cassiopeia A [17, 18]). The outer ejecta drive a shock wave through the CSM/ISM, heating the plasma to temperatures exceeding 10⁷ K.

The hot plasma resulting from the shock is at the outside bound by unshocked CSM/ISM, but at the inside by fast moving, cool ejecta. The high pressure in the shocked medium starts driving a shock wave back into the ejecta, thereby heating the ejecta. This shock is called the *reverse shock*. Note that the direction of the reverse shock in the frame of the observer depends on the evolutionary phase of the supernova remnant: initially the reverse shock is also moving outward at high speed, and the faster moving ejecta “bump” into the reverse shock. At a later stage, occurring when the swept up CSM/ISM mass exceeds several times the ejecta mass, the reverse shock moves in an opposite direction to the forward shock, i.e. it moves toward the center. Once it reaches the center, all ejecta have been shock heated and the core of the SNR is hot. Such a SNR can no longer be considered to be a *young* SNR, although some SNRs in this stage of the evolution still show evidence for highly metal enriched ejecta [e.g. the LMC remnant Dem L71 19, 20].

There are several analytic models for the shock structure and evolution of SNRs [21, 22, 23]. Fig. 1 shows the evolution of a SNR in a uniform ISM, as may be appropriate for Type Ia SNRs, which are thought not to have a strong stellar wind prior to explosion. The figure illustrates the behavior of the reverse shock, whose radius peaks, in this particular case, at around 1000 yr.

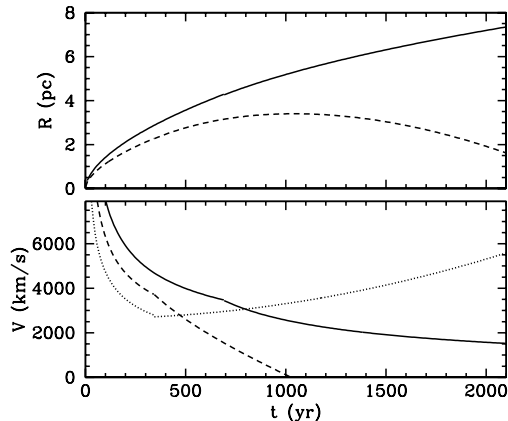


FIGURE 1. Shock radii and shock velocities as a function of time according to the Truelove-McKee $n = 7, s = 0$ model [22]. The solid line represents the forward shock, whereas the dashed line represents the reverse shock. In the bottom panel the reverse shock velocity in the frame of the ejecta is shown as a dotted line. The dimensionless model was adjusted to fit the properties of Kepler’s SNR [24].

The asymptotic behavior of the shock radius is that of the Sedov-Taylor self-similar evolution: i.e. :

$$R = \left(2.03 \frac{Et^2}{\rho_0}\right)^{1/5}, \quad V_s = \frac{dR}{dt} = \frac{2}{5} \frac{R}{t}, \quad (1)$$

with E the explosion energy, and ρ_0 the ISM density.

The medium surrounding a SNR can be rather complex. In particular, around core collapse supernovae one expects several regions shaped by different evolutionary stages of the progenitor. On the main sequence a massive star blows a fast ($v_w \sim 1000$ km s⁻¹), tenuous wind, but in the red supergiant phase a massive star loses mass with a rate of $\sim 10^{-4} - 10^{-5} M_\odot$, in a slow ($v_w \sim 10$ km s⁻¹) dense wind. Finally, the most massive stars may become Wolf-Rayet stars, which again have a very fast, tenuous wind. As a result the CSM may consist of several layers separated by shells caused by the interactions of winds from different phases in the star’s life.

If one considers an SNR evolving in a red supergiant (RSG) phase, which may be quite common, one expects the following density profile [21]:

$$\rho_{CSM} = \frac{\dot{M}}{4\pi r^2 v_w}. \quad (2)$$

The young SNR Cas A may be currently in this phase [25, 26]. The shock velocity in such a wind structure quickly follows the relation $V_s = \frac{2}{3} \frac{R}{t}$, which is indeed close to what is found for Cas A [27, 28].

Shock heating and temperature equilibration

The equations of mass-, momentum- and energy-flux conservation gives the following relation between shock velocity, V_s , and temperature for a high Mach number shock [e.g. 29]:

$$k\bar{T} = \frac{3}{16}\mu m_p V_s^2. \quad (3)$$

\bar{T} refers here to the average temperature, i.e. the average kinetic energy per particle. However, the microphysics of shock heating is not well known. SNR shocks are collisionless, which means that particle-particle collisions (Coulomb interactions) are rare, and insufficient to heat the plasma within a time comparable to the age of the SNR. Instead, the heating probably occurs through plasma waves. In such a case it is not quite known whether different particle species are heated to the same temperature. Alternatively, one may expect that all particle species have the same velocity distribution. This could arise if plasma waves in the shock scatter the incoming particles in different directions, with only small changes to the absolute velocities of the particles, which is V_s for all particles. In such a case the temperature for each particle species is different and scales with the mass, m_i , of the particle:

$$kT_i = \frac{3}{16}m_i V_s^2. \quad (4)$$

In the post-shock region, full equilibration will take place on a time scale of $\log(n_{et}) \approx 12.5$ [30], corresponding to $\sim 30,000$ yr of a typical density of $n_e \approx 1 \text{ cm}^{-3}$ (Fig. 2). Note that equilibration by particle-particle interactions depends on the charge of the particles and the mass ratio. For that reason electron-proton equilibration takes a long time, whereas proton-iron equilibration proceeds on a time scale of $\log(n_{et}) \approx 11.5$. The parameter n_{et} is also important for the ionization process, and can be directly measured using X-ray line ratios.¹

Electron temperature can be determined using X-ray spectroscopy, even employing CCD detectors. Ion temperatures can only be determined by measuring the thermal Doppler broadening of spectral lines. In order to eliminate Doppler broadening caused by line of sight motions due the SNR expansion, spectra should be obtained of the rim of a SNR, where only motions in the plane of the sky are to be expected. Most measurements of ion temperatures concern the hydrogen lines. Since hydrogen is quickly ionized, the hydrogen line emission

arises from very close to the shock front. The presence of hydrogen lines is only possible, if some neutral hydrogen is present in the ISM/CSM. The direct excitation in the post-shock gas gives rise to a narrow line, as the neutral hydrogen has not yet interacted with the shock heated plasma, and still has the temperature of the CSM. Charge exchange between an incoming neutral hydrogen atom and a proton in the heated gas, gives rise to a broadened line. The width of this broad component is a direct measurement of the proton temperature behind the shock [35, 36]. In the case of equilibration of temperatures, the proton temperature is equal to the mean plasma temperature.

X-ray spectroscopy, in general, provides a direct measure of the electron temperature. The electron temperature, together with n_{et} , determines the relative line ratios of lines of a given ion or atom. Also the characteristic cut-off in the bremsstrahlung continuum is directly related to the electron temperature. In young SNRs, however, synchrotron radiation is another source of continuum radiation, and the two mechanisms are not always easy to tell apart.

In principle, in X-rays one can also measure thermal Doppler broadening, but in practice the CCD detectors on board current X-ray observatories like Chandra and XMM-Newton pair great imaging capabilities with too poor spectral resolution to measure thermal Doppler widths. The high resolution grating spectrometers on board Chandra and XMM-Newton have a good spectral resolution, but they are slitless and the spectral quality is degraded for extended sources. Nevertheless, X-ray Doppler broadening has been measured for SN1006 using XMM-Newton's Reflective Grating Spectrometer [37]. This remnant has one of the lowest values of n_{et} : $n_{et} \approx 2 \times 10^9 \text{ cm}^{-3}\text{s}$. Optical, UV and X-ray spectroscopy of the northwestern part of this remnant reveals that ions, protons and electrons are out of temperature equilibrium [38, 39, 37], with the electrons being much cooler than the oxygen ions ($kT_e \approx 1.5 \text{ keV}$, $kT_{\text{OVI}} \approx 500 \text{ keV}$ [37]).

Apart from SN1006, also in several other SNRs have ion temperatures been measured, but only using optical and UV lines [40, 41, 42, 43]. Combining these measurements with electron temperatures obtained from X-ray spectroscopy shows that for the fastest shocks ($V_s > 1000 \text{ km s}^{-1}$) the electron temperature can be as low as 10% of the proton temperature. For the slow shocks, like in the Cygnus Loop, electrons and ions seem to be in full equilibrium, with a turnover from equilibrium to non-equilibrium occurring around 600 km s^{-1} [42]. Toward the end of this paper I will return to the issue of ion temperatures in the context of cosmic ray acceleration.

¹ I will skip the details here, but for those interested, more information and background can be found in [30, 31, 32, 33, 34].

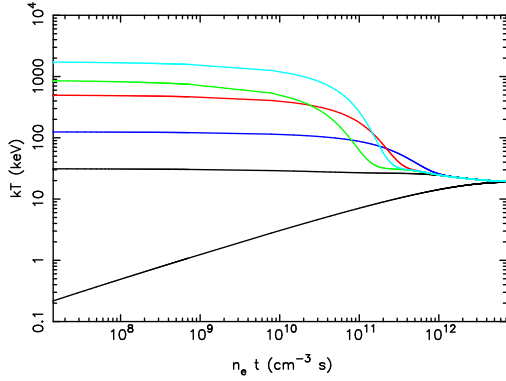


FIGURE 2. Theoretical model of the collisional equilibration process for a plane parallel shock model. It is assumed that the shock velocity is $V_s = 4000 \text{ km s}^{-1}$. The equilibration scales with the product of density and time, parameterized here as $n_e t$. The different lines indicate the temperature of different particle species. From bottom to top (on the left): electrons, protons, helium, oxygen, silicon, and iron.

MULTIWAVELENGTH IMPRINTS OF EFFICIENT COSMIC RAY ACCELERATION

The coming of age of TeV and X-ray astronomy over the last 15 years, has greatly increased our knowledge of cosmic ray acceleration by SNRs. Here I will explain some of the observations that form the basis of our current understanding. Not included here is TeV astronomy, which is amply addressed in other parts of these proceedings.

Measuring magnetic fields using X-ray synchrotron rims

The discovery by the ASCA satellite that the X-ray continuum emission from SN1006 is dominated by synchrotron emission [6],² has been the start of a number of discoveries in X-rays, which all relate to the cosmic ray acceleration properties of SNRs.

One of these discoveries is that the X-ray synchrotron emission from SNRs is confined to a region very close to the shock front. In the SNRs Cas A, Kepler (SN1604) and Tycho (SN1572), the synchrotron emission comes from a region only a few arcseconds near the shock front [47, 48]. In fact, the identification of the X-ray synchrotron emission required the superior angular resolu-

² This was anticipated by Reynolds & Chevalier [46].

tion of Chandra. In some other remnants, SN1006, RCW 86, RX J1713.7-3946, and RX J0852.0-4622, the X-ray synchrotron emission comes from a larger region, although some fine scale structure is present.

The size of the X-ray emitting region is now generally believed to be determined by the magnetic field strength. The lifetime of a relativistic electron in a magnetic field is in cgs units:

$$\tau_{loss} = \frac{637}{B_{\perp}^2 E} \text{ s.} \quad (5)$$

The typical photon energy E_{ph} corresponding to an electron energy E is:

$$E_{ph} = 7.4 E^2 B_{\perp} \text{ keV.} \quad (6)$$

The electrons are accelerated at the shock front by diffusive shock acceleration. At small scales their trajectories are determined by scattering on plasma waves (diffusion), but on large scales their average motion follows the plasma. If the shock compression ratio is $\chi \equiv \rho_0/\rho_1$, then the plasma velocity with respect to the shock is $V_1 = V_s/\chi$. As the electrons are moving slowly away from the shock front, they lose energy, until they are no longer emitting X-ray radiation. Thus, the loss time corresponds to the width of the X-ray emitting region through:

$$l_{loss} = \tau_{loss} \frac{1}{\chi} V_s. \quad (7)$$

By combining the measured width and the measured/inferred shock velocity with the observed photon energy one arrives at an estimate of the post-shock magnetic field strength [7], B , as illustrated in Fig. 3.

Several groups [49, 8, 50] do not use the loss length scale, l_{loss} , but instead assume that the length scale seen corresponds to the diffusion length scale, l_{diff} , i.e. the length scale at which diffusive motions are more important than the bulk plasma motion. However, in practice this method should give similar results, as long the synchrotron emission comes from electrons near the maximum acceleration energy, where diffusive acceleration is balanced by radiative losses, since $l_{diff} \leq l_{loss}$ for efficient acceleration [34, 51, 52].³

Magnetic field measurements of several SNRs have now been published, and indicate post-shock magnetic fields of 20 – 600 μG [7, 8, 53, 54, 9, 10, 55, 45]. This is higher than expected based on the compression of the average magnetic field in the ISM, $B \sim 5 \mu\text{G}$, and, therefore, suggests that some form of magnetic field amplifi-

³ Interestingly, the two methods have different assumptions: to estimate l_{diff} one has to assume Bohm-diffusion, whereas for estimating l_{loss} one has to assume a compression ratio. The fact that both methods give similar magnetic field values is an indication that both assumptions must be approximately valid [34].

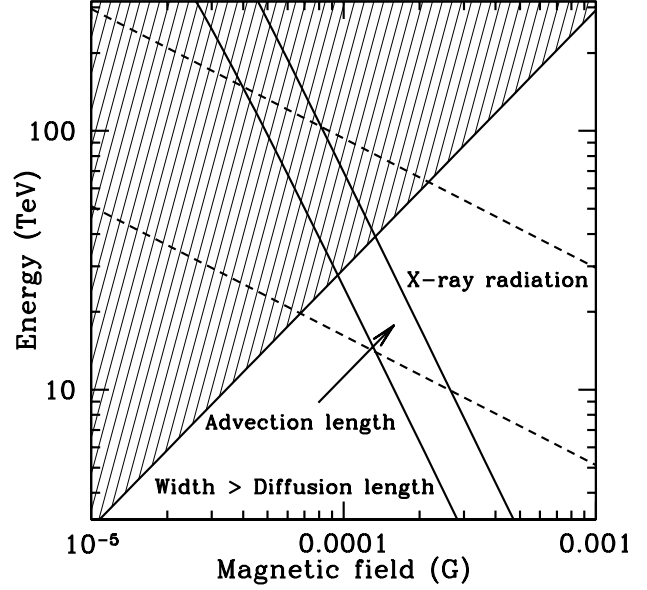
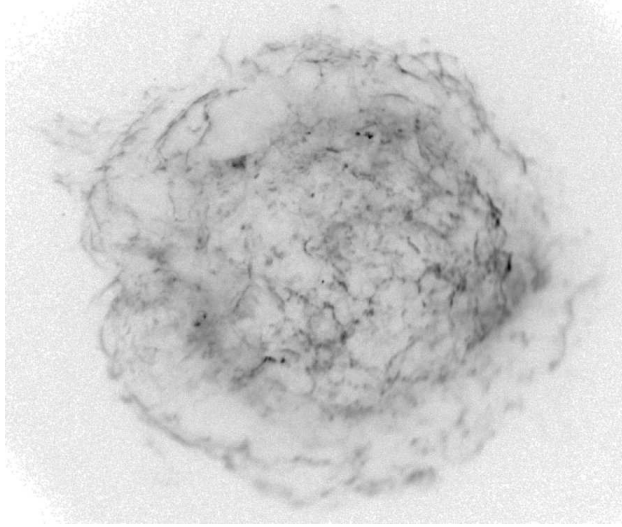


FIGURE 3. A deep Chandra image of Cas A [44] in the 4-6 keV continuum band (left). Note the thin filaments, marking the border of the remnant. The remnant has a radius of about $2.5'$. Right: The maximum cosmic ray electron energy versus magnetic field strength for the region just downstream of Cas A's shock front, as determined from the thickness of the filaments. The shaded area is excluded, because the filament width cannot be smaller than the minimum possible diffusion length [c.f. 7]. (These figures were published before in [45].)

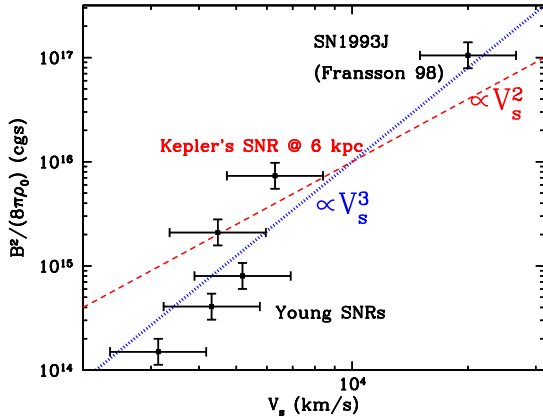


FIGURE 4. Dependence of the post-shock magnetic field energy density $B^2/(8\pi\rho_0)$ on the shock velocity V_s . The dashed line shows a V_s^2 dependency and the dotted line a V_s^3 dependency. The input values can be found in [45], except for SN1993J [56] and Kepler's SNR, for which the shock velocity in the southwest was taken from [24] and the density from [57].

cation mechanism is operating. The most likely mechanism is non-linear growth of plasma waves induced by streaming of cosmic rays [58, 11, 59], but some alternative, perhaps complementary, mechanisms have been proposed [60, 61].

Recently, high magnetic fields for SNRs were also reported based on small X-ray synchrotron brightness fluctuations in Cas A and RX J1713.7-3946 [62, 63, 64]. These findings support the presence of relatively high magnetic fields in young SNRs.

It is not yet clear what the relation is between the ram pressure at the shock front, $\rho_0 V_s^2$, and the post-shock magnetic field pressure. Based on observations it has been argued that $B^2 \propto \rho_0 V_s^2$ [54], whereas in [11] it has been argued that $B^2 \propto \rho_0 V_s^3$. In the latter case, a proportionally larger fraction of the incoming kinetic energy is transferred to cosmic rays and magnetic fields for during the earliest life of an SNR, since then the shock velocity is highest.

The problem with the current measurements of SNRs is that the dynamic range in density is quite high, but the dynamic range in shock velocity is small, since the magnetic fields can only be measured for X-ray synchrotron emitting remnants, and only SNRs with $V_s \gtrsim 2000 \text{ km s}^{-1}$ [65] are expected to emit X-ray synchrotron radiation, whereas most Galactic remnants known have $V_s < 5500 \text{ km s}^{-1}$. However, for supernova SN1993J, which has a shock velocity $\sim 20,000 \text{ km s}^{-1}$, a high magnetic field of 64 G has been reported [56]. If one assumes that for this object the same mechanism is at work, one may try to distinguish between the two magnetic field strength scalings. As Fig. 4 shows, including SN1993J favors a magnetic field strength scaling as

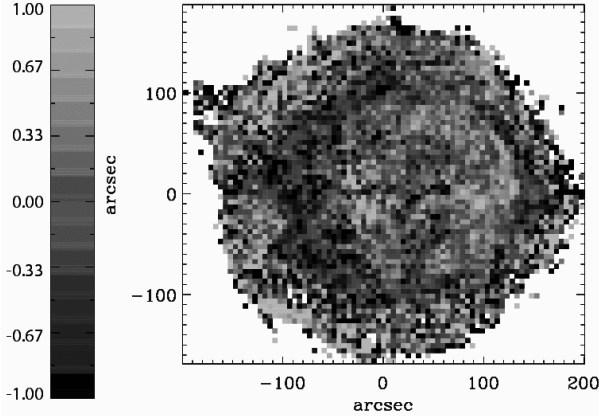


FIGURE 5. X-ray continuum spectral index map of Cas A based on the 1 Ms exposure by Chandra [66]. The gray scale coding indicates spectral number index with respect to $\Gamma = -3.1$. A hard spectral index (lighter pixels) is an indication for X-ray synchrotron emission. One sees here that hard spectral indices at the rims and in the central region, somewhat shifted to the west of the SNR. (Figure made by Eveline Helder, a color version can be found in [66].)

$B^2 \propto \rho_0 V_s^3$, but one should regard this with some caution, since the magnetic field in SN1993J may have different origin than the magnetic fields in young SNRs.

Magnetic field amplification at the reverse shock

The high magnetic field of SN1993J raises the question how universal magnetic field amplification is. Does it require certain preconditions, like a medium strength magnetic field, to start with?

Interestingly, it was recently reported that for the young SNR Cas A a large part of the X-ray synchrotron emission is coming from the reverse shock, in particular in the western region of Cas A [66, 63] (Fig. 5).

In the past, reverse shocks as sites of particle acceleration were often ignored (but see [67, 68]), since it was assumed that the magnetic field in the ejecta was low, due to their large scale expansion. However, particle acceleration at the reverse shock, sufficiently fast to give rise to X-ray synchrotron emission, may be important for two reasons: 1) it shows that magnetic field amplification is rather universal, and that it does not require relatively large initial magnetic fields 2) some cosmic rays may be accelerated from metal rich material, which could lead to signatures in the cosmic ray composition. Indeed there is some evidence that 20% of the Galactic cosmic rays come from massive stars [69, 70].

As remarked by Luke Drury at the symposium, one should not overestimate the significance of the reverse

shock for their contribution to the observed cosmic ray spectrum: cosmic ray acceleration is efficient when the physical shock velocity is high. For the reverse shock this occurs when the shock starts to move back toward the center of the SNR, until it reaches the center. This is a relatively short period in the life of a SNR. Moreover, during this time the area spanned by the reverse shock is smaller than that of the forward shock, so the total number of particles entering the reverse shock is much less than the number of particles swept up by the forward shock. Both these aspects are illustrated in Fig. 1. For Cas A it is believed that the reverse shock velocity in the frame of the freely expanding ejecta is less than 2000 km s^{-1} [23], except in the western region, where somehow the reverse shock is almost at a standstill in our frame, and the ejecta are shocked with the ejecta free expansion velocity of $4000 - 8000 \text{ km s}^{-1}$ [66].

What is the maximum energy cosmic rays can be accelerated to?

Several authors have pointed out that the high magnetic fields that have been inferred from X-ray synchrotron emitting rims indeed allow protons to be accelerated to $> 10^{15} \text{ eV}$, and heavy ions can in principle be accelerated to even higher energies [e.g. 34, 51]. It is also clear that the magnetic field energy density scales with:

$$B^2 \propto \rho_0 V^\alpha, \quad (8)$$

with $\alpha = 2$ or 3 . As a consequence higher magnetic fields are present early in the life of a SNR when the shock velocity is higher. This has led to the suggestion that the highest energy cosmic rays are accelerated early on, and, as the magnetic field drops, those particles escape first. The peak energy is thus a function of time. The observed cosmic ray spectrum is in such a scenario a superposition of cosmic rays released over an extended period of time [71]

Note that not only does the magnetic field energy depend on V_s , but also on ρ_0 . This means that the highest energies are reached for shocks in dense environments. Some supernovae have by their very nature high circumstellar densities. As indicated by Eq. 2, the density around a massive, wind blowing star, is highest for slow wind speeds, v_w , and high mass loss rates. So it is likely that the highest cosmic ray energies are obtained by SNRs developing in a RSG wind. An example, as mentioned above, is Cas A. In fact, an optical spectrum of the light echo of the supernova explosion reveals that it is the remnant of a Type IIb supernova, very similar to the bright radio supernova SN1993J [72]! Cas A's progenitor probably had only a very short Wolf-Rayet star phase, if any at all [25, 73, 26].

An SNR like Cas A reaches the self-similar shock evolution very early on, in which case $R_s \propto t^{2/3}$ and $V_s \propto t^{-1/3}$ [21]. One can use this similarity evolution to estimate the maximum proton cosmic ray energy as a function of time: First note that $E_{max} \propto t_{acc} B_1 V_s^2$, with t_{acc} the acceleration time, for which we can take the age of the SNR. Using Eq. 2 and Eq. 8 one finds:

$$B_1 \propto \frac{1}{R_s} t^{-\alpha/6} \propto t^{-2/3-\alpha/6}. \quad (9)$$

We therefore find for the maximum proton energy in a young SNR evolving in a dense stellar wind:

$$E_{max} \propto t^{1-4/3-\alpha/6}, \quad (10)$$

for $\alpha = 3$ this means $E_{max} \propto t^{-5/6}$, and for $\alpha = 2$ this is $E_{max} \propto t^{-2/3}$.

The value for the magnetic field found for Cas A ($B \approx 0.5$ mG) is sufficient for E_{max} presently to be $\sim 10^{15}$ eV. However, Cas A's ability to accelerate cosmic rays was probably even better in the past: according to Eq. 10 and using $\alpha = 3$, when Cas A was only 30 yr old the maximum proton energy was $E_{max} \sim 7 \times 10^{15}$ eV and its post-shock magnetic field strength 7 mG. Note that the evolution of the magnetic field ensures that the diffusion length scale (assuming Bohm diffusion) does not exceed the size of the remnant, since B evolves faster with t than R_s . The $1/r^2$ density profile makes that the flux of particles does not depend on the shock radius.

All this implies that probably most of the Galactic cosmic rays with $E > 10^{15}$ eV were accelerated by Type II/Type IIb supernova remnants, during the first 100 yr of their lives. Most massive stars explode while in their RSG phase. Only stars more massive than $25 M_\odot$ (a minority), probably explode in the Wolf-Rayet stars phase. Their SNRs are probably less capable of acceleration cosmic rays to very high energies, unless they explode with larger energies, as in the case of hypernovae.

Measuring compression ratios using X-ray imaging

Magnetic field amplification is probably a result of cosmic ray streaming. The presence of relatively large magnetic fields in young SNRs, therefore, implies by itself efficient cosmic ray acceleration. I use the word "efficient" here in contrast to fast acceleration. Fast acceleration means that cosmic rays are accelerated to high energies, efficient that the cosmic ray content of SNRs is energetically important.

Efficient cosmic ray acceleration affects both the evolution of the SNR itself [74], and the cosmic ray spectrum [75, 76, 77]. If cosmic ray acceleration is very efficient the cosmic rays provide back-pressure to the unshocked plasma, which gives rise to a concave spectrum,

i.e. it is steeper than the test particle spectrum at low energies and flatter at high energies. If the internal energy of the post-shock gas is dominated by *relativistic* cosmic rays the compression ratio increases. A standard high Mach number shock in a monatomic gas ($\gamma = 5/3$) will have a compression ratio of $\chi = (\gamma + 1)/(\gamma - 1) = 4$, whereas for a gas dominated by relativistic particles ($\gamma = 4/3$) this is $\chi = 7$. Compression ratios in excess of 7 are possible, if energy losses are taken into account.

In old SNRs radiative energy losses lead to higher compression ratio, since shock velocities of $V_s \lesssim 200$ km s⁻¹, produce plasma with a temperature of $< 10^6$ keV, near the peak of the cooling curve. This gives rise to the formation of the filamentary structures radiating in forbidden lines, which make for beautiful Hubble Space Telescope images, of SNRs like Vela, the Cygnus Loop or, N49.

For young SNRs, which efficiently accelerate cosmic rays, energy may leak out of the plasma due to the escape of cosmic rays. The highest energy cosmic rays are the most likely ones to escape. Escaping cosmic rays are only energetically important for flat, or concave spectra. In that case the highest energy cosmic rays may contain a significant fraction of the total internal plasma energy. Although concave spectra are expected in most efficient cosmic ray acceleration models, this is by no means a certainty yet; see the contribution by V. Zirakashvili in these proceedings.

Higher compression ratios due to cosmic ray escape will give rise to different ratios of the forward and reverse shock radii or of the forward shock and contact discontinuity radii [74], the contact discontinuity being the boundary between shocked supernova ejecta and shock heated CSM.

Indeed, for both Tycho's SNR [55] and SN1006 [78] it has been reported that the contact discontinuity lies very close to the forward shock. SN1006, a newly detected H.E.S.S. source, is an interesting SNR in this respect, since the X-ray synchrotron emission, and also most of the radio emission, is confined to the northeastern and southwestern regions. If we take the shocks in these regions sites of efficient cosmic ray acceleration, one may expect that in those regions the contact discontinuity and forward shock are closer to each other than in the rest of the remnant, due to a higher compression ratio. This is indeed what is found, but surprisingly also in the other regions of SN1006 the contact discontinuity is closer to the forward shock than expected [78].

This suggests that apart from a higher compression ratio also some other mechanisms (e.g. ejecta clumping, hydrodynamical instabilities) are at play in bringing the ejecta close to the shock front. So SNR morphology hints at high compression ratios, signifying efficient cosmic ray acceleration, but a quantitative results cannot yet be obtained.

Radio polarimetry and magnetic field amplification

Fast cosmic ray acceleration requires a small diffusion constant, for which, apart from a relatively high magnetic field, also a turbulent magnetic field is required, i.e. $\delta B/B \sim 1$. Magnetic field amplification by growth of plasma waves due to streaming instabilities [11], naturally provides both the magnetic field strength and its turbulence. Observationally, turbulent magnetic fields are implied by the fact that near the maximum electron energies the diffusion length scale and advection (loss time) length scales are similar (see [34] and above).

Other evidence that the magnetic fields are turbulent comes from the long known observations of radio polarization of SNRs. These indicate that old SNRs have preferentially tangential magnetic fields, whereas young SNRs have radial magnetic fields [79]. Some recent results regarding magnetic field structure can be found for Cas A [47], Kepler's SNR [80], RCW 86 [81] and the old SNR PKS 1209-51 [82].

The tangential magnetic fields in old SNRs are caused by the compression of the ISM magnetic fields, which have some large scale coherence (see the contribution by R. Beck in this volume). Shocks only compresses the tangential component of the field. In those regions where the uncompressed magnetic fields are perpendicular to the shock normal, the post-shock magnetic field will be enhanced, increasing the radio brightness of these regions.

The radial magnetic fields in young SNRs are not that easily explained by MHD simulations [83, 84]. Rayleigh-Taylor instabilities at the contact discontinuity, indeed, produce radial magnetic fields [83]. However, near the shock front, simulations produce tangential, not radial magnetic fields. Efficient cosmic ray acceleration, may indeed be the missing ingredient. This can happen in two ways. First of all, efficient cosmic ray acceleration gives rise to turbulent magnetic fields. Since these have no preferred direction, strong tangential fields where the shock normal is perpendicular to the magnetic fields are avoided [84]. Secondly, enhanced shock compression will bring the Rayleigh-Taylor instabilities closer to the shock front [85]. However, it is not clear whether the compression is sufficiently enhanced to indeed produce radial magnetic fields close to the forward shock. Zirakashvili reported at this symposium that MHD simulations incorporating magnetic field amplification tends to make the downstream magnetic field stretch in a radial direction [59].

It, therefore, seems likely that the observed radial magnetic field structure in young SNRs is either facilitated or a direct by-product of efficient cosmic ray acceleration and magnetic field amplification.

High resolution spectroscopy and cosmic ray acceleration efficiency

In the literature on thermal Doppler broadening of lines from SNRs, one has concentrated mostly on the equilibration of electrons and ions, and the consequences for deriving shock speeds using Eq. 3 or Eq. 4. Rarely has the discussion focussed on the influence of cosmic rays on the measured temperatures. However, cosmic rays may contain a large part of the internal energy, and change the adiabatic index of the plasma. These effects are not taken into account in Eqs. 3, 4, which are usually used to derive shock parameters.

An exception is the case of the Small Magellanic Cloud remnant 1E 0102.2-7219. As reported in [86] the electron temperature of this remnant is too cold compared to the measured shock velocity, even allowing for non-equilibration of electron and ion temperatures. A direct measurement of the ion temperature in this remnant is difficult, as this oxygen rich remnant does not emit optical hydrogen lines.

How much does efficient cosmic ray acceleration influence the post-shock plasma temperatures? The answer depends on two parameters 1) the fraction of the pressure contributed by non-thermal components, 2) the energy escape fraction associated with cosmic rays. For a strong shock one can parameterize these with:

$$w \equiv \frac{P_{NT}}{P_T + P_{NT}}, \quad (11)$$

the relative pressure of the non-thermal components (cosmic rays and magnetic fields) [c.f. 87, 77], and the shock compression ratios, which for a strong shock is:

$$\chi = \frac{G + \sqrt{G^2 - (1 - \epsilon_{esc})(2G - 1)}}{1 - \epsilon_{esc}}, \quad (12)$$

with ϵ_{esc} the fraction of the incoming energy flux that is taken away from the shock by cosmic rays, and $G \equiv \frac{3}{2}w + \frac{5}{2}$.⁴ One can apply these expressions to the following relation between plasma temperature and shock temperature:

$$kT_i = (1 - w) \frac{1}{\chi} \left(1 - \frac{1}{\chi}\right) V_s^2, \quad (13)$$

which is a generalized version of Eq. 4, as can be seen by inserting $w = 0$ and $\chi = 4$. Eq. 13 and 12 are graphically depicted as a function of w and ϵ_{esc} in Fig. 6.

It is clear from these equations that high resolution spectroscopy offers the opportunity to learn about the internal energy budget of the plasma. Measuring kT_p and V_s

⁴ I assume here that the non-thermal contributions to the pressure have an adiabatic index of $\gamma = 4/3$.

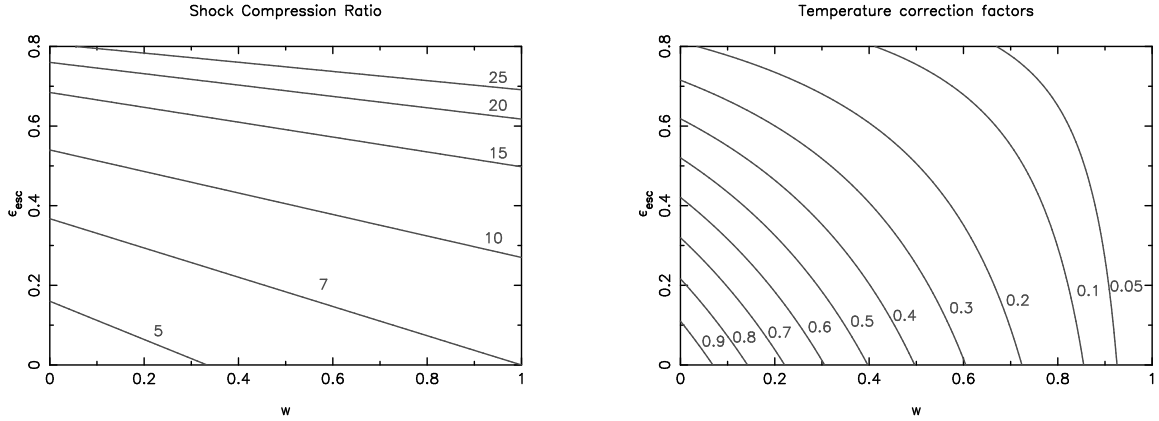


FIGURE 6. Graphical representation of the effects of cosmic ray escape and relative cosmic ray pressure (w) on the compression ratio (left) and the post-shock temperature (right). In the right hand figure, the values are given as correction factors with respect to the standard strong shock expressions (Eq. 3,4).

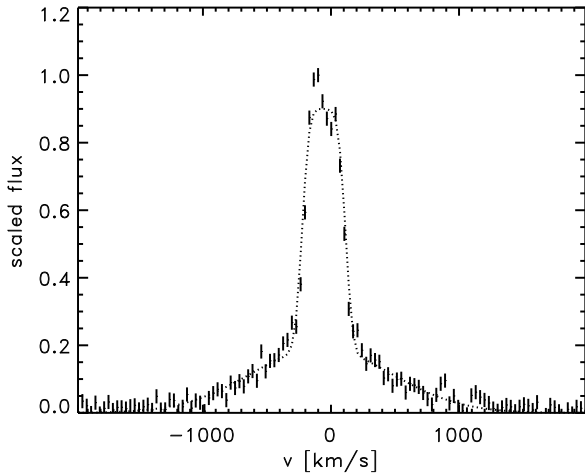


FIGURE 7. $H\alpha$ line profile of the northeastern part of RCW 86, as observed with the VLT (Helder et al. in preparation). The line consists of a narrow peak, from direct excitation, and broad wings caused by charge exchange between the incoming neutral hydrogen atoms and the shock heated protons. The FWHM of the broad wing is a direct measure of the proton temperature. The narrow peak is broadened due to the relatively broad line spread function (LSF) of 330 km s^{-1} . Preliminary results give a FWHM of $(1270 \pm 60) \text{ km s}^{-1}$, after correction for the LSF. (Figure provided by E. Helder)

independently gives a handle on cosmic ray acceleration efficiencies. This should be combined with a measurement of kT_e in order to test for ion-electron equilibration. Ideally, one would like to measure also the compression factor independently, in order to alleviate the degeneracy between w and ϵ_{esc} . On the other hand, it seems unlikely that $w < \epsilon_{esc}$, which constrains part of the degeneracy.

So far the interpretation of most measurements of kT using optical, UV and X-ray spectroscopy have ignored the role of cosmic ray physics (but see [88]). To some extent this seemed unnecessary, because spectra were taken from locations from which no strong X-ray synchrotron radiation is emitted, like the northwestern region of SN1006. The northwestern region of SN1006 has bright $H\alpha$ emission, which made it easy to obtain high quality spectra. The X-ray synchrotron regions, on the other hand, only show weak $H\alpha$ emission. That is unfortunate, since at these synchrotron rims cosmic ray acceleration is likely to be more efficient. It is not quite clear whether the lack of $H\alpha$ emission from the X-ray synchrotron rims is a coincidence. Three possible reasons for this anti-correlations are 1) the presence of neutral hydrogen damps plasma wave, decreasing the efficiency for cosmic ray acceleration [89]; 2) cosmic rays diffusing away from the shock ionize the CSM, suppressing the number of neutral hydrogen atoms entering the shock; 3) bright $H\alpha$ emission comes from the densest regions, but as a result of the higher density the shock velocity has decelerated, thereby diminishing the acceleration efficiency [52].

Knot g in Tycho's SNR

A case in point is the $H\alpha$ -bright “Knot g” in Tycho’s SNR. The broad $H\alpha$ line component gives a proton temperature of $5.9 \pm 0.9 \text{ keV}$, indicating a shock velocity of $1700\text{-}2200 \text{ km s}^{-1}$, depending on whether ion-electron equilibration is assumed or not. The average shock velocity of Tycho’s SNR is 3100 km s^{-1} , based on radio proper motion studies [90], and assuming a distance of 2.5 kpc.

Without cosmic ray acceleration the expected temperature is $kT_p = 19$ keV for an unequilibrated plasma, or $kT = 11$ keV for an equilibrated plasma. However, for “knot g” the shock velocity is probably much lower, since the radio proper motion at this location indicates an expansion parameter $V_s/(R_t/t) \approx 0.25$, rather than the 0.46 found in the rest of the remnant. The reason is probably that the blast wave at “knot g” is encountering dense material slowing down the shock, but also resulting in bright $H\alpha$ emission. For the lower expansion velocity of “knot g” the measured plasma temperature is consistent with a shock without cosmic ray modification. This is at odds with the above mentioned findings that all over this remnant the contact discontinuity is too close to the forward shock as a result of cosmic ray acceleration [55]: cosmic rays do not seem to contribute much to the internal energy in “knot g”.

The low plasma temperature in LMC SNR 0509-67.5

One of the fastest expanding young SNRs is 0509-67.5 in the Large Magellanic Cloud. This remnant has an age of about 400 yr [45, 91] and high resolution X-ray spectroscopy with XMM-Newton’s RGS experiment shows line broadenings of $\sigma_v \approx 5000$ km s⁻¹, which is dominated by kinematic Doppler broadening, as the whole SNR is observed [92]. The broadening provides a lower limit to the shock velocity, since the plasma velocity directly behind the shock is $3/4V_s$, and most of the line emission comes from the reverse shock region, which moves probably 30% slower than the plasma immediate downstream of the shock velocity. This means that the shock velocity is at least $V_s \approx 6700$ km s⁻¹, but likely larger than $V_s \approx 8000$ km s⁻¹. The hydrogen line broadening has been measured to be 3710 ± 400 km s⁻¹ (FWHM) [43], implying a proton temperature of $kT_p = 26$ keV. This translates into a shock velocity 3000 – 5400 km s⁻¹, which is much lower than the actual shock velocity. The ratio of the measured temperature and the expected temperature is ~ 0.2 (for $V_s \approx 8000$ km s⁻¹), indicating, according to Fig. 6, either a high partial pressure not coming from the thermal plasma, $w = 0.7$, or a combination of lower w with a relatively high cosmic ray escape fraction. Our knowledge of cosmic ray acceleration in 0509-67.5 would be more complete, if either X-ray synchrotron emission or TeV γ -rays would be detected. Unfortunately, for the moment the remnant is too distant to identify X-ray synchrotron emission from the shock front.

The plasma temperature in an X-ray synchrotron emitting region in RCW 86

Ideally one would like to measure post shock temperatures of region that emit both X-ray synchrotron radiation and/or TeV γ -rays. In the future this can be undertaken with the next generation of high resolution, imaging X-ray spectrometers, as are planned for the Japanese NEXT mission or the ESA/NASA/JAXA International X-ray Observatory (IXO). X-ray and UV spectroscopy have advantages over $H\alpha$ spectroscopy, since X-ray line emission does not require a partially neutral pre-shock gas.

In the mean time one has to concentrate on the faint $H\alpha$ line emission coinciding with X-ray synchrotron emission. In a new study Helder et al. (in preparation) have done that for the SNR RCW 86, the possible remnant of AD 185 [93]. RCW 86 has recently been detected in TeV γ -rays by H.E.S.S. (Hoppe et al. these proceedings). Its X-ray emission is a mix of X-ray synchrotron, and thermal radiation. The X-ray emission indicates strong density contrasts, and probably also strong gradients in shock velocities along the shell [52]. $H\alpha$ emission has been detected all around the shell [94], but the $H\alpha$ emission is weak in the northeastern side, where, the emission is dominated by X-ray synchrotron radiation. As a consequence ESO’s Very Large Telescope is needed to obtain $H\alpha$ spectroscopy of this region (Fig. 7 shows the preliminary spectrum). Surprisingly, the line width is 1270 km s⁻¹ (FWHM), corresponding to a proton temperature of $kT_p = 3$ keV, (ignoring proton-electron equilibration). This is much larger than in other parts of RCW 86, where typically line width of 500 km s⁻¹ are found [41], but it is smaller than expected for an X-ray synchrotron emitting shock for which $V_s > 2000$ km s⁻¹ [65]. The plasma temperature appears to be too low, which can be explained, if cosmic rays have taken up part of the shock energy. For a reasonable value of $V_s \approx 2500$ km s⁻¹, Fig. 6 suggests $w = 0.6$ for an escape fraction of $\epsilon_{esc} = 0$.

However, an alternative scenario to explain the low plasma temperature in RCW 86 is that the X-ray synchrotron emitting electrons were accelerated in the past, when the shock velocity was higher. This requires a long loss time for the electrons, corresponding to a relatively low magnetic field. Indeed, the value for the magnetic field derived from the X-ray emitting region is $24\mu\text{G}$ [52], corresponding to a sufficiently long loss time of ~ 500 yr. The new H.E.S.S. results are in agreement with such a low magnetic field, provided that the TeV emission has a leptonic, rather than a hadronic origin.

So, unfortunately, no clear cut answer can be given about the cosmic ray content of RCW 86, as long as the shock velocity is not directly measured, or the γ -ray

emission process is identified. However, RCW 86 illustrates how seemingly remote areas of astrophysics, γ -ray astronomy and optical spectroscopy, are both needed to obtain answers about cosmic ray acceleration efficiencies.

SUMMARY AND CONCLUSION

The topic of these proceedings is γ -ray astrophysics, a field of astrophysics that is still relatively young, but has already changed our perception of cosmic ray acceleration in SNRs. However, as I have indicated here, more traditional fields of astronomy valuable clues about cosmic ray acceleration in young SNRs, as well.

In reality, not all signatures of cosmic ray acceleration are unambiguous. For example, the evidence for high compression ratios is tantalizing [55, 78], but the high compression ratios all over the remnants, even those region where cosmic ray acceleration seems not to be efficient, is confusing, and requires further investigation. However, it is important that we know now for what kind of multiwavelength signatures of cosmic ray acceleration to look, and what kind of observations are needed to make further progress.

Comparing our current knowledge of cosmic ray acceleration by young SNRs with what was known a decade ago, one sees that a lot of observational progress has been made. My guess is that most cosmic ray physicists are a much more optimistic about the idea that young SNRs are the sources of cosmic rays up to the “knee” than 15 years ago.

ACKNOWLEDGMENTS

I thank Eveline Helder and Klara Schure for helpful discussions and providing me with material for this review. I thank the organizers for inviting me to this interesting symposium, and I acknowledge helpful and lively discussions with Vladimir Zirakashvili, Luke Drury, and Tony Bell. The author is supported by a Vidi grant from the Netherlands Science Foundation (NWO).

REFERENCES

1. M. Renaud, et al., *ApJ* **647**, L41–L44 (2006).
2. C. Badenes, E. Bravo, and J. P. Hughes, *ApJ* **680**, L33–L36 (2008).
3. P. O. Lagage, and C. J. Cesarsky, *A&A* **125**, 249–257 (1983).
4. J. S. Shklovsky, *Supernovae*, Interscience Monographs and Texts in Physics and Astronomy, London: Wiley, 1968, 1968.
5. J. A. Esposito, S. D. Hunter, G. Kanbach, and P. Sreekumar, *ApJ* **461**, 820 (1996).
6. K. Koyama, et al., *Nat* **378**, 255 (1995).
7. J. Vink, and J. M. Laming, *ApJ* **584**, 758–769 (2003).
8. E. G. Berezhko, L. T. Ksenofontov, and H. J. Völk, *A&A* **412**, L11–L14 (2003).
9. A. Bamba, et al., *ApJ* **621**, 793–802 (2005).
10. J. Ballet, *astro-ph/0503309* (2005).
11. A. R. Bell, *MNRAS* **353**, 550–558 (2004).
12. A. Aharonian, F. Akhperjanian, J. Barrio, et al., *A&A* **370**, 112–120 (2001).
13. F. A. Aharonian, et al., *Nat* **432**, 75–77 (2004).
14. F. Aharonian, et al., *A&A* **437**, L7–L10 (2005).
15. J. Albert, et al., *A&A* **474**, 937–940 (2007).
16. Y. M. Butt, T. A. Porter, B. Katz, and E. Waxman, *MNRAS* **386**, L20–L22 (2008).
17. P. O. Lagage, A. Claret, J. Ballet, F. Boulanger, C. J. Cesarsky, D. Cesarsky, C. Fransson, and A. Pollock, *A&A* **315**, L273–L276 (1996).
18. J. Rho, T. Kozasa, W. T. Reach, J. D. Smith, L. Rudnick, T. DeLaney, J. A. Ennis, H. Gomez, and A. Tappe, *ApJ* **673**, 271–282 (2008).
19. K. J. van der Heyden, J. A. M. Bleeker, J. S. Kaastra, and J. Vink, *A&A* **406**, 141–148 (2003).
20. J. P. Hughes, P. Ghavamian, C. E. Rakowski, and P. O. Slane, *ApJ* **582**, L95–L99 (2003).
21. R. A. Chevalier, *ApJ* **258**, 790–797 (1982).
22. J. K. Truelove, and C. F. McKee, *ApJS* **120**, 299–326 (1999).
23. J. M. Laming, and U. Hwang, *ApJ* **597**, 347–361 (2003).
24. J. Vink, *ArXiv e-prints* **803** (2008).
25. R. A. Chevalier, and J. Oishi, *ApJ* **593**, L23–L26 (2003).
26. K. M. Schure, J. Vink, G. García Segura, and A. Achterberg, *ApJ* **686**, 399 (2008).
27. J. Vink, H. Bloemen, J. S. Kaastra, and J. A. M. Bleeker, *A&A* **339**, 201–207 (1998).
28. T. Delaney, and L. Rudnick, *ApJ* **589**, 818 (2003).
29. Y. Zeldovich, and Y. P. Raizer, *Elements of gasdynamics and the classical theory of shock waves*, New York: Academic Press, 1966, edited by Hayes, W.D.; Probstein, Ronald F., 1966.
30. H. Itoh, *PASJ* **29**, 813–830 (1977).
31. E. Gronenschild, and R. Mewe, *A&AS* **48**, 305–331 (1982).
32. J. P. Hughes, and D. J. Helfand, *ApJ* **291**, 544–560 (1985).
33. K. J. Borkowski, W. J. Lyerly, and S. P. Reynolds, *ApJ* **548**, 820–835 (2001).
34. J. Vink, “Non-thermal X-ray Emission from Supernova Remnants,” in *AIP Conf. Proc. 745: High Energy Gamma-Ray Astronomy*, edited by F. A. Aharonian, H. J. Völk, and D. Horns, 2005, pp. 160–171.
35. R. A. Chevalier, R. P. Kirshner, and J. C. Raymond, *ApJ* **235**, 186–195 (1980).
36. K. Heng, M. van Adelsberg, R. McCray, and J. C. Raymond, *ApJ* **668**, 275–284 (2007).
37. J. Vink, J. M. Laming, M. F. Gu, A. Rasmussen, and J. Kaastra, *ApJ* **587**, 31–34 (2003).
38. P. Ghavamian, P. F. Winkler, J. C. Raymond, and K. S. Long, *ApJ* **572**, 888–896 (2002).
39. J. C. Raymond, W. P. Blair, and K. S. Long, *ApJ* **454**, L31–L37 (1995).
40. R. C. Smith, J. C. Raymond, and J. M. Laming, *ApJ* **420**, 286–293 (1994).

41. P. Ghavamian, J. Raymond, R. C. Smith, and P. Hartigan, *ApJ* **547**, 995–1009 (2001).
42. P. Ghavamian, J. M. Laming, and C. E. Rakowski, *ApJ* **654**, L69–L72 (2007).
43. P. Ghavamian, W. P. Blair, R. Sankrit, J. C. Raymond, and J. P. Hughes, *ApJ* **664**, 304–321 (2007).
44. U. Hwang, et al., *ApJ* **615**, L117–L120 (2004).
45. J. Vink, “X-ray High Resolution and Imaging Spectroscopy of Supernova Remnants,” in *The X-ray Universe 2005, ESA SP-604 Vol. 1, A. Wilson ed. (ESA, ESTEC, The Netherlands)*, 2006, p. 319.
46. S. P. Reynolds, and R. A. Chevalier, *ApJ* **245**, 912 (1981).
47. E. V. Gotthelf, et al., *ApJ* **552**, L39–L43 (2001).
48. U. Hwang, A. Decourchelle, S. S. Holt, and R. Petre, *ApJ* **581**, 1101–1115 (2002).
49. A. Bamba, R. Yamazaki, M. Ueno, and K. Koyama, *Adv. Space Research* **33**, 376–380 (2004).
50. E. G. Berezhko, G. Pühlhofer, and H. J. Völk, *A&A* **400**, 971–980 (2003).
51. E. Parizot, A. Marcowith, J. Ballet, and Y. A. Gallant, *A&A* **453**, 387–395 (2006).
52. J. Vink, J. Bleeker, K. van der Heyden, A. Bykov, A. Bamba, and R. Yamazaki, *ApJ* **648**, L33–L37 (2006).
53. E. G. Berezhko, and H. J. Völk, *A&A* **419**, L27–L30 (2004).
54. H. J. Völk, E. G. Berezhko, and L. T. Ksenofontov, *A&A* **433**, 229–240 (2005).
55. J. S. Warren, et al., *ApJ* **634**, 376–389 (2005).
56. C. Fransson, and C.-I. Björnsson, *ApJ* **509**, 861–878 (1998).
57. G. Cassam-Chenaï, et al., *A&A* **414**, 545–558 (2004).
58. A. R. Bell, and S. G. Lucek, *MNRAS* **321**, 433–438 (2001).
59. V. N. Zirakashvili, V. S. Ptuskin, and H. J. Völk, *ApJ* **678**, 255–261 (2008).
60. A. M. Bykov, and I. N. Toptygin, *Astronomy Letters* **31**, 748–754 (2005).
61. J. Giacalone, and J. R. Jokipii, *ApJ* **663**, L41–L44 (2007).
62. D. J. Patnaude, and R. A. Fesen, *AJ* **133**, 147–153 (2007).
63. Y. Uchiyama, and F. A. Aharonian, *ApJ* **677**, L105–L108 (2008).
64. Y. Uchiyama, F. A. Aharonian, T. Tanaka, T. Takahashi, and Y. Maeda, *Nat* **449**, 576–578 (2007).
65. F. A. Aharonian, and A. M. Atoyan, *A&A* **351**, 330–340 (1999).
66. E. A. Helder, and J. Vink, *ApJ* **686**, 1094 (2008).
67. J. Rho, K. K. Dyer, K. J. Borkowski, and S. P. Reynolds, *ApJ* **581**, 1116–1131 (2002).
68. D. C. Ellison, A. Decourchelle, and J. Ballet, *A&A* **429**, 569–580 (2005).
69. M. E. Wiedenbeck, and D. E. Greiner, *Physical Review Letters* **46**, 682–685 (1981).
70. W. R. Binns, M. E. Wiedenbeck, M. Arnould, A. C. Cummings, G. A. de Nolfo, S. Goriely, M. H. Israel, R. A. Leske, R. A. Mewaldt, E. C. Stone, and T. T. von Rosenvinge, *New Astronomy Review* **52**, 427–430 (2008).
71. V. S. Ptuskin, and V. N. Zirakashvili, *A&A* **429**, 755–765 (2005).
72. O. Krause, S. M. Birkmann, T. Usuda, T. Hattori, M. Goto, G. H. Rieke, and K. A. Misselt, *Science* **320**, 1195– (2008).
73. P. A. Young, et al., *ApJ* **640**, 891–900 (2006).
74. A. Decourchelle, D. C. Ellison, and J. Ballet, *ApJ* **543**, L57–L60 (2000).
75. D. C. Ellison, and S. P. Reynolds, *ApJ* **382**, 242–254 (1991).
76. E. G. Berezhko, and D. C. Ellison, *ApJ* **526**, 385–399 (1999).
77. P. Blasi, S. Gabici, and G. Vannoni, *MNRAS* **361**, 907–918 (2005).
78. G. Cassam-Chenaï, J. P. Hughes, E. M. Reynoso, C. Badenes, and D. Moffett, *ApJ* **680**, 1180–1197 (2008).
79. J. R. Dickel, and D. K. Milne, *Australian Journal of Physics* **29**, 435–460 (1976).
80. T. DeLaney, B. Koralesky, L. Rudnick, and J. R. Dickel, *ApJ* **580**, 914–927 (2002).
81. J. R. Dickel, R. G. Strom, and D. K. Milne, *ApJ* **546**, 447–454 (2001).
82. D. K. Milne, and R. F. Haynes, *MNRAS* **270**, 106 (1994).
83. B.-I. Jun, and M. L. Norman, *ApJ* **472**, 245 (1996).
84. K. M. Schure, J. Vink, A. Achterberg, and R. Keppens, *Rev Mex AA (in press)* (2008).
85. J. M. Blondin, and D. C. Ellison, *ApJ* **560**, 244–253 (2001).
86. J. P. Hughes, C. E. Rakowski, and A. Decourchelle, *ApJ* **543**, L61–L65 (2000).
87. R. A. Chevalier, *ApJ* **272**, 765–772 (1983).
88. C. E. Rakowski, J. M. Laming, and P. Ghavamian, *ApJ* **684**, 348–357 (2008).
89. L. O’Drury, P. Duffy, and J. G. Kirk, *A&A* **309**, 1002–1010 (1996).
90. E. M. Reynoso, D. A. Moffett, W. M. Goss, G. M. Dubner, J. R. Dickel, S. P. Reynolds, and E. B. Giacani, *ApJ* **491**, 816 (1997).
91. A. Rest, et al., *Nat* **438**, 1132–1134 (2005).
92. D. Kosenko, J. Vink, S. Blinnikov, and A. Rasmussen, *A&A in press* (2008).
93. F. R. Stephenson, and D. A. Green, *Historical supernovae and their remnants*, Oxford: Clarendon Press, 2002.
94. R. C. Smith, *AJ* **114**, 2664 (1997).